Transport and escape in a deformable channel driven by fractional Gaussian noise

Ruoxing Mei[*]
Department of Applied Mathematics, Northwestern Polytechnical University, Xi'an 710072, China

Yong Xu[†]
Department of Applied Mathematics, Northwestern Polytechnical University, Xi'an 710072, China
and MIIT Key Laboratory of Dynamics and Control of Complex Systems, Northwestern Polytechnical University, Xi'an 710072, China

Jürgen Kurths[‡]
Potsdam Institute for Climate Impact Research, Potsdam 14412, Germany

(Received 20 February 2019; revised manuscript received 26 June 2019; published 12 August 2019)

Fractional Gaussian noise (FGN) with the Hurst exponent H is an important tool to model various phenomena in biophysical systems, like subdiffusion in a single protein molecule. Considering that there also exists a confined structure which can be modeled as a channel in these systems, transport and escape driven by FGN in a deformable channel are investigated in this paper. By calculating the mean velocity, and the mean first passage time (MFPT) for crossing the nearest bottleneck and the probability distribution of the final position, effects of FGN and channel structure on the system dynamics are illustrated. Our results indicate that FGN has a complex influence mechanism under different combinations of H and the noise intensity. For a persistence case ($H > 0.5$), the mean velocity decreases but MFPT increases with the increase of the noise intensity and H. While for an antipersistence case ($H < 0.5$), when H is small, the relationships among the mean velocity, MFPT and the noise intensity are exactly the opposite to persistence cases. When H has a large value, the mean velocity tends to first decrease and then increase. Moreover, effects of the bottleneck and channel asymmetry are investigated. It is shown that a small H and a large channel width can lead to a large mean velocity and fast crossing. Besides, a channel asymmetry can affect the system dynamics by inducing asymmetric structure and adjusting the width of bottleneck. However, the effect of the bottleneck is the main factor. Therefore, a combination of channel with wide bottleneck and FGN in an antipersistence regime is the optimal choice to promote the transport and escape. These results provide a basis for the explanation of molecular activity in living organisms and the design of particle mixture separators.

DOI: 10.1103/PhysRevE.100.022114

I. INTRODUCTION

Many processes from chemistry to biology can be modeled as dynamical systems influenced by noise. Typically, noise is often assumed as Gaussian white noise. Under this assumption, a system has a normal diffusion which satisfies a linear time dependence relationship between its mean-square displacement (MSD) and time, i.e., $\langle x^2(t)\rangle \propto t$, where $\langle x^2(t)\rangle$ means the MSD, $\propto$ is a linear relationship. Besides, in several systems ranging from biology to soft matter, there also exist other types of anomal diffusion obeying the relationship $\langle x^2(t)\rangle \propto t^{2H}$, $H \neq 0.5$, where H called Hurst exponent. Examples are motion in crowded biological cell environment like the cytoplasm and plasma membrane in living cells [1–4], active motion in biological cells [5], diffusion of lipids in bilayers [6] and lipid granule motion at longer times [7], subdiffusive motion of bacterial chromosomal loci [8], the tracer spreading and diffusion in living cells [9,10], single particle tracking in micellar solutions [11], and also the diffusion of a single-file [12] and a viscoelastic medium with a broad range of coupling strengths [13]. In these cases, fractional Gaussian noise (FGN) with the Hurst exponent H becomes a more prominent model to characterize the noise. FGN was found by Kolomogorov first and then reintroduced by Mandelbrot and Van Ness [14]. After that, more and more studies focused on FGN and obtained a variety of results. Basing on the properties of FGN, Wood, Lowen, and others proposed various methods to generate the corresponding random numbers [15–19]. Kou *et al.* explained the subdiffusion of a single protein molecule successfully by introducing FGN into a generalized Langevin equation [20–22]. Pei and Xu studied the averaging principles for some kinds of stochastic differential equations with Markov switching processes driven by fractional Brownian motion (FBM), which is the formally integration of FGN, and proved the existence and uniqueness of solutions [23–25]. Deng and Zhu investigated linear and nonlinear oscillators under FGN with $H \in (0.5, 1)$ [26]. In addition, the first passage time in an open wedge domain or absorbing boundaries, Kramer's-like escape in linear Langevin equation with a harmonic potential and stochastic resonance in a bistable potential are investigated in some degree [27–31].

[*]ruoxing_mei@yahoo.com
[†]Corresponding author: hsux3@nwpu.edu.cn
[‡]kurths@pik-potsdam.de

With the deepening of relevant studies on microscale, confined structures are gradually found in systems obeying anomal diffusion. Examples are transport of particles in biological cells, ion channels and reactions in porous media [32–34]. It has been confirmed that confinement has nonnegligible effects on system behaviors [35]. For this condition, results in an opening environment without boundary confinement are not sufficient. Therefore, transport and diffusion in a confined environment become more appropriate and attractive. To investigate the effect of confinement, Jacobs *et al.* proposed a theoretical analysis method to systems with periodic channels from the diffusion equation and Gibbs entropy respectively, and gave a Fick-Jacobs (FJ) equation to characterize the probability density evolution of particles in a confined environment [36–39]. After this, scholars began to study systems consisting of confined spaces from various aspects. Some studies focused on the influences of force and noise in the presence of a confined channel. For example, Palmeri found the inhibitory effect of noise on the effective diffusion in a channel, which opened the door to directed transport in molecular motors [40]. Wu found the multiple inversion of the moving direction caused by a transverse ac force [41]. Others mainly studied behaviors of particles with various radius and shapes. For instance, Riefler *et al.* found that particles with a large radius have a small current [42]. Li *et al.* studied the transport of particles with different sizes in an asymmetric channel, and developed a new method to separate particles by directing them to opposite directions [43]. These results are important for the design and realization of fine separation. Some investigations referred on the geometry of confinement. Ao studied the rectification of Brownian motion in left-right and upside-down asymmetric channels [44]. Wang studied the biased transport in a corrugated channel with a constant width but a varying centerline [45]. Ding *et al.* turned their focus to time changing boundaries [46], which promote a better interpretation for life activities in living organisms. Researches on other channels, like a pulsation channel, are also gradually unfolding [47]. However, all these studies viewed the system noise as independent Gaussian white noise. Only a few articles concerned the correlation and large jump of noise in actual systems. For example, Ai studied the rectified transport in a periodic channel driven by FBM and Lévy flight without any external forces, and found a directed transport induced by the spectral distribution of FBM and the nonthermal character of Lévy noise [48]. Xu investigated effects of Gaussian colored noise, and discovered the enhancement of the suitable noise correlation time [49].

In this paper, we mainly study influences of FGN and the structure of a deformable channel on three indexes, including the mean velocity, the distribution of the final position and the first passage time for crossing the nearest bottleneck. The paper is arranged as follows. The motion equation of particles, the deformable channel, a detailed introduction about FGN, and definitions of the three indexes are presented in Sec. II. Effects of the Hurst exponent and the noise density of FGN on the three indexes are investigated in Sec. III. Influences of a deformable channel mainly consisting of the bottleneck and asymmetry, are discussed in Sec. IV.

II. MODEL DESCRIPTION

We consider the transport and escape of particles in a deformable channel under the influence of FGN. In this section, a detailed description to the model discussed here and the three main factors to be concerned about, namely, the dynamical equation of particles (Sec. II A), FGN (Sec. II B), and the deformable channel (Sec. II C), are presented. The dynamical equation of particles in a free environment can be described by a Langevin equation. The deformable channel, denoted by $w(x)$, possesses a periodically varying cross section and reflecting boundaries.

A. Langevin equation

Under the assumption of overdamped conditions, the Langevin equation obeys

$$\frac{dx(t)}{dt} = F + \sqrt{D}\xi_x^H(t), \tag{1}$$

$$\frac{dy(t)}{dt} = \sqrt{D}\xi_y^H(t), \tag{2}$$

where $[x(t), y(t)]$ determines the position of the particles at time t. F is a constant external force along the axial direction of the deformable channel. In our study, it is set to be 1. $\xi_x^H(t)$ and $\xi_y^H(t)$ are two independent FGN with the same noise intensity D in x and y axis, respectively. Generally, $\xi_x^H(t)$ and $\xi_y^H(t)$ can be seen as the formally derivation of a FBM, which is denoted as $B_H(t)$. Relationships and properties of $B_H(t)$, $\xi_x^H(t)$, and $\xi_y^H(t)$ are given in Sec. II B.

B. FBM and FGN

For the FBM $B_H(t)$, by virtual of a long memory, it has become a powerful tool to study practical phenomena in systems like biology, physics and soft matter since being proposed by Kolomogorov. When $B_H(t)$ is standard, it is a stationary Gaussian process with zero-initial value, zero-mean, Hurst exponent H, and autocorrelation function

$$\langle B_H(t)B_H(s)\rangle = \tfrac{1}{2}[t^{2H} + s^{2H} - |t-s|^{2H}]. \tag{3}$$

When $H = 0.5$, correlation function becomes into $\langle B_H(t)B_H(s)\rangle = \min(t, s)$, and $B_H(t)$ corresponds to a normal unit Brownian motion. For $H \neq 0.5$, $B_H(t)$ has two important properties, self-similarity and stationary increment, which are very useful in the analytical and numerical research on systems driven by FBM. For self-similarity, it means

$$\{B_H(ct)\} \Longleftrightarrow c^H\{B_H(t)\}, \tag{4}$$

where " $\Longleftrightarrow$ " means that processes in the two sides have the same probability density distribution, c is an arbitrary constant. The stationary increment satisfies

$$\{B_H(t+\Delta t) - B_H(t)\} \Longleftrightarrow \{B_H(s+\Delta t) - B_H(s)\}, \quad \forall \Delta t, t, s > 0, \tag{5}$$

where Δt is the time difference that can be any constant value. This property Eq. (5) means that the distribution of the increment only depends on Δt, regardless of the start time.

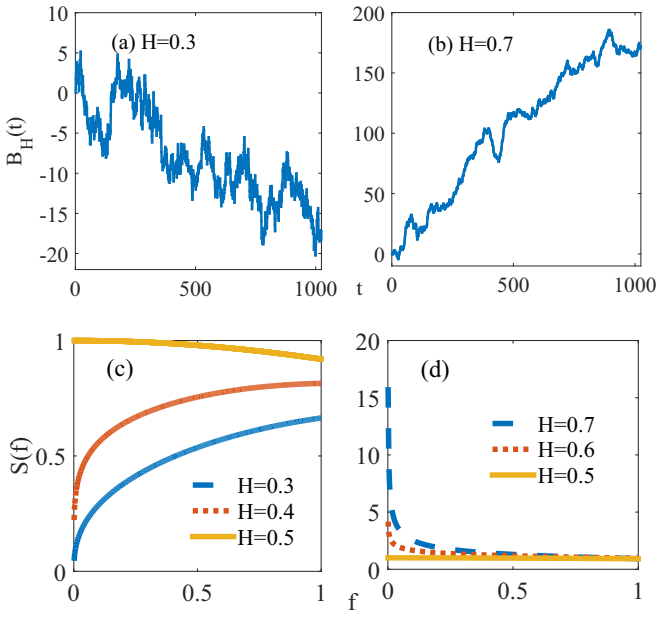

FIG. 1. Samples of FBM and spectral density $S(f)$ for different H. (a) Sample of FBM for $H = 0.3$; (b) sample of FBM for $H = 0.7$; (c) $S(f)$ for antipersistence cases $H = 0.3$ and 0.4; (d) $S(f)$ for persistence cases $H = 0.6$ and 0.7.

As is well known, FGN can be viewed as the formally derivation of FBM. Thus, taking $\xi_x^H(t)$ as an example, it can be rewritten as

$$\xi_x^H(t) = \frac{dB_H(t)}{dt} = \frac{B_H(t+\Delta t) - B_H(t)}{\Delta t}. \tag{6}$$

Then, according to Eqs. (3) and (6), one can obtain the autocorrelation function $r(t)$ of $\xi_x^H(t)$, satisfying

$$\begin{aligned} r(t-s) &= \langle \xi_x^H(t)\xi_x^H(s)\rangle \\ &= \tfrac{1}{2}[(t-s)+\Delta t]^{2H} + \tfrac{1}{2}|(t-s)-\Delta t|^{2H} \\ &\quad - |t-s|^{2H}, \quad \forall t > s. \end{aligned} \tag{7}$$

From the perspective of a discrete integer time, $r(t)$ can be changed into

$$\begin{aligned} r(j-i) &= \langle \xi_x^H(i)\xi_x^H(j)\rangle \\ &= \tfrac{1}{2}[(j-i)+1]^{2H} + \tfrac{1}{2}|(j-i)-1|^{2H} \\ &\quad - |j-i|^{2H}, \quad \forall j > i, \end{aligned} \tag{8}$$

where i and j are positive integers. In the long-time limit, the autocorrelation function Eq. (7) decays as

$$r(t) = \langle \xi_x^H(t)\xi_x^H(0)\rangle \sim 2H(2H-1)t^{2H-2}. \tag{9}$$

When $0 < H < 0.5$, the process is called antipersistence case. In this situation, the prefactor $2H - 1$ in Eq. (9) is negative. Hence, the two adjacent steps in a FGN sample are negatively correlated, which means that the direction of one step is opposite to its previous step. Thus, as a sum of FGN sample, the corresponding FBM is more random [see $H = 0.3$ in Fig. 1(a)]. When $0.5 < H < 1$, the process is the persistence case. Then, the prefactor in Eq. (9) is positive. The direction at two adjacent moments tend to be the same, resulting into a smoother FBM sample [see $H = 0.7$ in Fig. 1(b)]. By performing a Fourier transform on the correlation function Eq. (7), the spectral density $S(f)$ of $\xi_x^H(t)$ can be obtained as

$$S(f) = 2\sin(\pi H)\Gamma(2H+1)(1-\cos f)[|f|^{-2H-1} + B(f,H)], \tag{10}$$

where $B(f,H) = \sum_{j=1}^{\infty}\{(2\pi j+f)^{-2H-1} + (2\pi j - f)^{-2H-1}\}$, and f is the frequency. From the spectrum Eq. (10), we can get a more intuitive comprehension to the sample path of FGN, as shown in Figs. 1(c) and 1(d). For $H < 0.5$ [see Fig. 1(c)], when f increases, $S(f)$ also increases, which means that the high-frequency components in the FGN sample are larger than the low-frequency ones. Besides, at the same f value, the high-frequency components decrease for increasing H. While for $H > 0.5$ [see Fig. 1(d)], with the increase of f, $S(f)$ decreases, which means that there are more lower frequency components in the FGN sample. For a fixed f, the larger H, the bigger $S(f)$, and the more low-frequency components [50].

Considering the self-similarity and stationary increment of FBM, a simulation of the Langevin Eqs. (1) and (2) can be realized through the following discrete form:

$$\begin{aligned} x(i+1) &= x(i) + F\,dt + \sqrt{D}(dt)^H \xi_x^H(i), \\ y(i+1) &= y(i) + \sqrt{D}(dt)^H \xi_y^H(i), \end{aligned} \tag{11}$$

where dt is the time step, $\xi_x^H(i)$ and $\xi_y^H(i)$ are FGN random numbers, and $[x(i), y(i)]$ is the position of the particle at the ith step. The methods used in this paper to generate $\xi_x^H(i)$ and $\xi_y^H(i)$ are from references [16,17]. Detailed steps are given in the Appendix.

C. Deformable channel

Compared with a free environment, the existence of a channel changes the available spaces for the system, intervenes and regulates the motion trajectory of particles reaching the channel boundary. Thus, one can say that the channel geometry is an important factor to regulate particle transport and escape. To explore the effect mechanism, this paper chooses a deformable channel $w(x)$, which is expressed by the following function:

$$w(x) = \pm a\left[\sin(2\pi x) + \frac{\Delta}{4}\sin(4\pi x)\right] \pm b. \tag{12}$$

Here, Δ and b are parameters to determine the shape of the channel. For Δ, it affects the symmetry of $w(x)$. When $\Delta = 0$, $w(x)$ is symmetric, whereas a nonzero Δ generates an asymmetric channel (see the left panel in Fig. 2). To clearly explain the relationship between the asymmetry of $w(x)$ and Δ, two symbols L_l and L_r are introduced. L_l represents the length between one maximum of $w(x)$ and its adjacent minimum in the left side. L_r is defined as the length to the adjacent minimum in the right side. When $\Delta < 0$, $L_l > L_r$. The left side of $w(x)$ is flat and the right side is steep. When $\Delta > 0$, $L_l < L_r$. The left side of $w(x)$ is steep and the right side is flat. Besides, as Δ changes, the minimum width of the channel also varies. Generally, the part with the minimum width in the channel can be regarded as a bottleneck. Correspondingly,

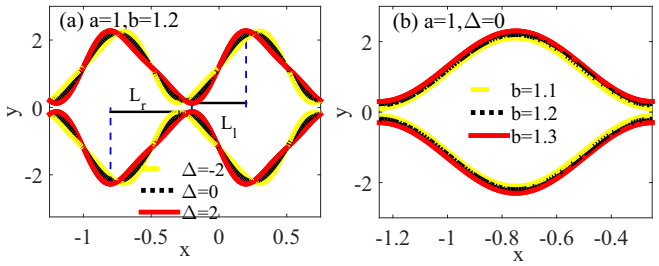

FIG. 2. Schematic diagram of the deformable channel $w(x)$ for different parameters.

the value of the minimum part is the width of the channel bottleneck. The schematic diagram of Fig. 2(a) indicates that the bottleneck for $\Delta \neq 0$ is narrower than that for $\Delta = 0$. As $|\Delta|$ increases, the width of the bottleneck becomes smaller and smaller. In addition, b also contributes to the width of the bottleneck, which is shown in the right figure. Equation (12) demonstrates that b equals to the distance of the vertical movement along the y axis. For fixed Δ and a, the width changes with b. A large b leads to a larger width. In this paper, b is called the width parameter and Δ the asymmetry parameter.

When there is no $w(x)$, particles can move in its adjacent surrounding. However, when $w(x)$ exists, the behavior is different. Walls of $w(x)$ will restrict the particles within its inside. To clarify the influence of the channel walls on the transport, an elastic reflection boundary condition is added to the walls. Under this condition, when the particles arrive the walls of $w(x)$, a collision process between them occurs, as shown in Fig. 3. Assume that the position $[x(i), y(i)]$ (square point 1 in Fig. 3) of the particle is inside the $w(x)$, and the position $[x'(i+1), y'(i+1)]$ (circle point 2 in Fig. 3) calculated according to Eq. (11) at the next step located outside the $w(x)$. The line between points 1 and 2 is the original trajectory, and the tangent of $w(x)$ at the intersection P (diamond point in Fig. 3) is the reflecting surface. In the collision process, the particles will perform a reflecting trajectory from point P to point 3, which is symmetric with the line between points P and 2. The length of the reflection trajectory is equal to the distance between points P and 2. Point 3 with position $[x(i+1), y(i+1)]$ is the position after the collision which is actually

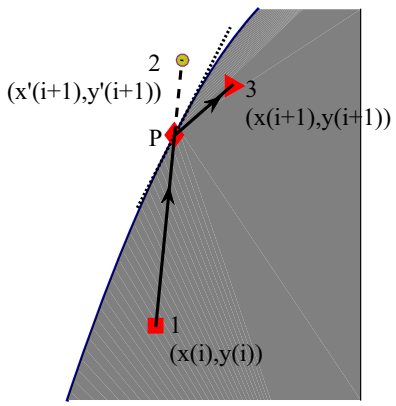

FIG. 3. Schematic diagram of the collision process between particles and walls of $w(x)$ under the elastic reflection condition.

used in our study. In summary, the reflection boundary of $w(x)$ changes the original trajectory of the particles, controls the direction and distance of the reflection, and thus affects the actual displacement of the particle in each dt.

To illustrate the influence mechanisms of FGN and the deformable channel on the system behaviors, three indexes are mainly calculated in this paper. The first one is mean velocity v, defined as

$$v = \lim_{t\to\infty} \frac{1}{N} \sum_{n=1}^{N} \frac{x_n(t) - x_n(t_0)}{t - t_0}, \tag{13}$$

where t_0 is the initial time, N is the realized sample number, $x_n(t)$ means the particle position of the nth realization at time t.

The second index is the mean first passage time (MFPT). Roughly speaking, it refers to the time the particles cost to reach a specified location from its initial position. Here, the MFPT we considered means that particles starting from the initial position $x_n(t_0)$ moving until crossing the nearest channel bottleneck. The corresponding expression is written as

$$\frac{1}{N} \sum_{n=1}^{N} [\inf\{t > 0 \mid x_n(t) \geqslant x_r \text{ or } x_n(t) \leqslant x_l, \\ x_n(s) \in (x_l, x_r), \forall s < t\}],$$

where inf is the infimum. x_r and x_l represent the positions of the nearest bottleneck in the right and left sides, respectively. For systems driven by FGN, like transport in a harmonic or symmetric truncated potential, there exist analytical results between MFPT and H [28,29]. However, due to the space confinement induced by $w(x)$ in our model, these analytical results are not suitable. Therefore, numerical results about the MFPT are given.

The third index is the density distribution P_{st} of the final position $\{x_n(t)\}_{1\leqslant n\leqslant N}$ as t tends to infinity. Here, the symbols

$$PA = \min\{x_n(t)\}_{1\leqslant n\leqslant N}, \quad PB = \max\{x_n(t)\}_{1\leqslant n\leqslant N},$$

are first introduced. Then, P_{st} can be approximated as

$$P_{\text{st}}(m) = \frac{\sum_{n=1}^{N} \chi_{\{x_n(t)\in \text{Par}(m)\}}}{Nd}, \quad m = 1, 2, \ldots, M, \tag{14}$$

where M is the number of partitions of the interval $[PA, PB]$ which is set to be 20. d is the class interval, satisfying

$$d = \frac{PB - PA}{M}.$$

Par(m) is the mth interval in the partition with form $[PA + (m-1)d, PA + md)$. χ is the indicator function.

III. INFLUENCES OF NOISE

Noise is an important factor to adjust dynamical behaviors in random systems. When noise is modeled as FGN, most results focus on the effects of FGN under open areas. In this section, the influence mechanisms of FGN parameters D and H in a confinement are mainly calculated. In the calculation process, the time step is $dt = 10^{-3}$. The realized sample numbers are $N = 10^4$ and the total integration number

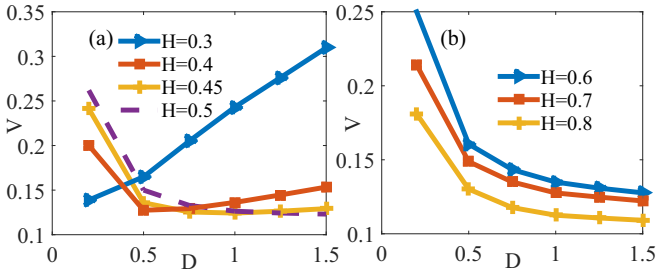

FIG. 4. Influences of D on the mean velocity v for different H.

is more than 10^6 in each sample. Other system parameters are $\Delta = 0$, $a = 1$, $b = 1.02$.

A. Influences of noise intensity D

At first, the influences of D on v are investigated. It was proved that under a Gaussian white noise, which also corresponds to our result in $H = 0.5$, an increase of D contributes to a decrease of v because of the increased collisions between particles and channel walls. However, in the antipersistence case, an increasing intensity D leads to novel changes of v. As illustrated in Fig. 4(a), for $H = 0.3$, as D increasing, v also increases and gradually exceeds the result in $H = 0.5$. That is, a large noise intensity in $H = 0.3$ promotes the particle transport. However, when H changes from 0.3 to 0.5, this promoting effect disappears at small D. When D increases to a certain threshold, this promoting effect appears again, but very weak. Specifically, for $H = 0.4$, an increase of $D \in [0.2,\ 0.5)$ leads to a rapid decrease of v, which is always smaller than the case $H = 0.5$. As D continues to increase from 0.5, it becomes to enlarge v and larger than for $H = 0.5$ at $D \geqslant 0.9$. For the case $H = 0.45$, the promoting mechanism disappears within a wide range of D. v keeps smaller than for $H = 0.5$ at any $D < 1.1$. Thus, the threshold of D that inhibit a particle transport increases as H is increasing. While in the persistence case, the influence mechanism is simper than for $H < 0.5$, as shown in Fig. 4(b). A larger D leads to a smaller v. Noise with large intensity prevents a particle transport monotonically. In addition, as D increases from 0.2 to 1, v drops rapidly, i.e., the inhibitory effect of D on the particle transport is obvious. When D increases from 1, the decline rate of v is so small that the inhibitory effect can be ignored.

Here, a supplementary explanation to the results in Fig. 4 is given. When D approaches 0, v in Figs. 4(a) and 4(b) does not approach 0. The reasons for this phenomenon are as follows. Three factors that affect v are discussed in our model, i.e., the boundary of $w(x)$, FGN and the external force F. For the boundary of $w(x)$, it is elastically reflective. This means that the particles reaching the boundary will be intercepted, returning to the inside of $w(x)$ and continuing to move. So, it can be ruled out that the particles are absorbed by the boundary. For FGN, D determines the density of the excitation. The larger the D, the larger the displacement of the particles in each step. For F, it is fixed as $F = 1$, which means that it will always push the particles to move to the right. Therefore, when these three factors work together, even if $D \sim 0$, F will promote the transport, ensure that the particles are not absorbed, and lead to a nonzero v.

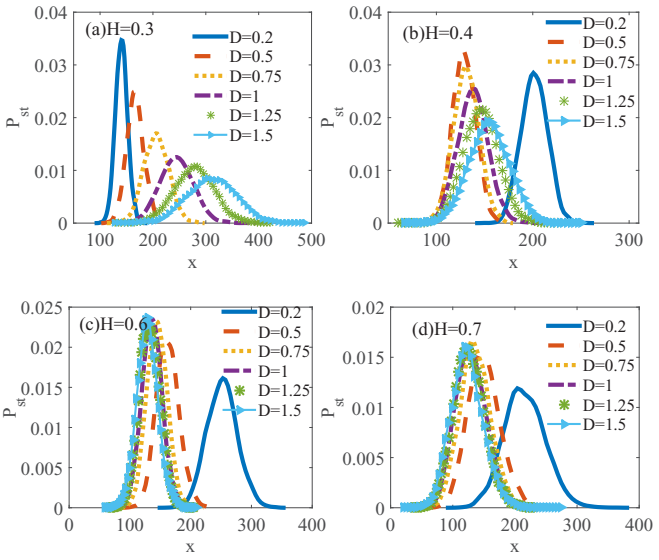

FIG. 5. P_{st} of the final positions of particles for different D.

According to the definition Eq. (13), for each trajectory, its velocity is determined by the differences between the initial and the final position at an infinity time interval. In our calculation, the initial position $x_n(0)$ of all samples is kept the same. Therefore, it can be considered that v is only related to the final position of the particles. For a more thorough analysis about the influence mechanism of D on v, P_{st} under different D is studied and plotted in Fig. 5.

Figures 5(a) and 5(b) show P_{st} in antipersistence cases. As presented for every H and D, the corresponding P_{st} shows a bell-shape with a maximum. Meanwhile, under different H, with the increase of D, the peak of P_{st} shifts in different directions and distances. For $H = 0.3$, as D changes in [0.5, 0.75, 1, 1.25, 1.5], P_{st} moves to right at a constant speed and the shifting distance of the peak caused by each increase of D keeps almost the same. This means a linear relationship between D and v in Fig. 4(a). While for $H = 0.4$, the shifting direction changes as D varying from 0.2 to 1.5. When $D = 0.2$, most particles locate in the position around 200. When $D = 0.5$, particles cannot move a long distance, but just arrive at the position around 130. This results into a huge left directed shift for the peak of P_{st} and contributes to the sharp decrease of v at the same time. When D continues to increase from 0.5, the peak of P_{st} shifts to the right monotonically. And per shifting the distance is no more than 20. Therefore, the corresponding v increases slowly. In summary, Figs. 5(a) and 5(b) explain and verify the phenomena in Fig. 4(a). Figures 5(c) and 5(d) are P_{st} in persistence cases. As shown, when $H = 0.6$, the peak of P_{st} shifts from 250 to 150 as D is changing from 0.2 to 0.5. Then, when D continues to increase, the peak still shifts to the left. But each shifting distance is getting smaller, and eventually disappears. Similarly, when $H = 0.7$, P_{st} presents a similar trend. These results verify the conclusions in Fig. 4(b).

The narrow escape is an important and interesting question in nonequilibrium systems, like transistors, fine separation and the protein valves of biological membranes [51]. Particle transports through a narrow bottleneck can be seen as a narrow escape, too. In Fig. 6(a), influences of D on the MFPT is

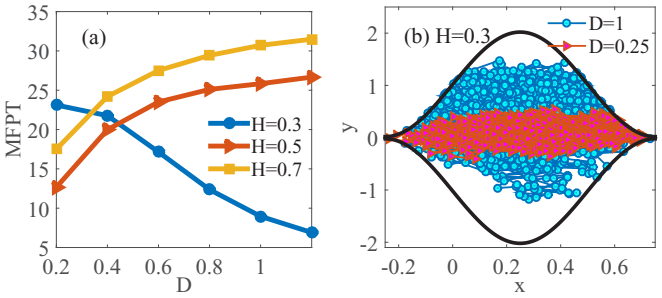

FIG. 6. (a) Relations between the MFPT and D for different H. (b) The single trajectory of particles when escaping from the bottleneck for $D = 0.25$ and 1.

investigated. Relationships between them are different for various values of H. For $H = 0.3$, an increase of D results into a decrease of MFPT. This means that, the noise intensity has a promoting effect on crossing the bottleneck. To illustrate the influences of D more clearly, single trajectories for $H = 0.3$ under different D are given in Fig. 6(b). In both cases $D = 1$ and $D = 0.25$, it is clear that the particles have to travel the space between the two bottlenecks in one cell before escaping from one side or the other. However, when $D = 1$, the displacement at each single step in the trajectory is larger, while for $D = 0.25$ the displacement is smaller. Under this case, the time a particle takes to escape for $D = 0.2$ is longer than for $D = 1$. This verifies the phenomenon in Fig. 6(a) that the MFPT decreases as D increases for $H = 0.3$. Meanwhile, from the definitions of v and MFPT, one can guess that the relation between D and MFPT is opposite to D and v. As shown in case $H = 0.7$, MFPT is becoming bigger as D is increasing, while the corresponding v will become small. In actual systems, basing on results obtained in this section, appropriate parameters can be selected to satisfy the requirements. For example, in a fine separation, a rapid separation in a short time can greatly save costs, so a combination of "small H, large D" or "small D, large H" should be selected. Table I summarizes the main findings of this part.

B. Influences of Hurst exponent H

For FBM/FGN, the Hurst exponent H is an important parameter. It determines the self-similarity, correlation function, and spectral density. Any changes of H can lead to interesting statistical properties for samples of FBM/FGN and then affect the transport properties of stochastic dynamic systems driven by FGN eventually. This has been reflected in Sec. III A. In Fig. 4(a), there are some intersections between curves, which are indicating complex influence mechanisms of H. In this

TABLE I. Summary of the influence of increased D on v, P_{st}, and MFPT for different H.

	v	The peak of P_{st}	MFPT
$H = 0.3$	Increase	Move to the right	Decrease
$H = 0.4$	Increase first, then decrease	Move to the right first, then to the left	
$H \geqslant 0.5$	Decrease	Move to the left	Increase

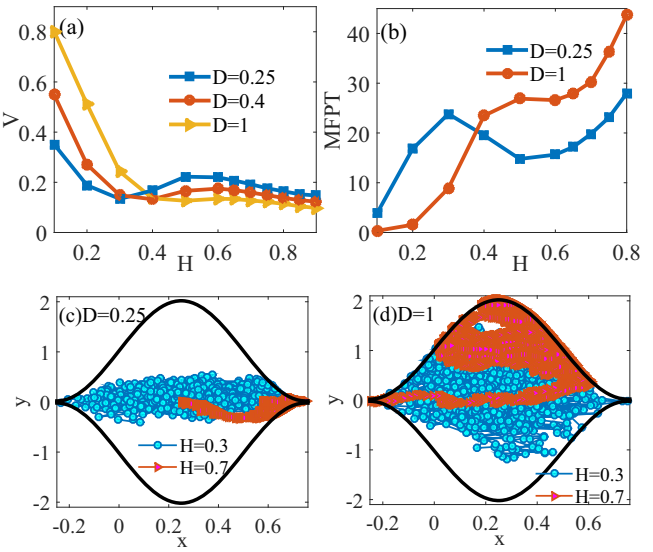

FIG. 7. (a) Influences of H on v for different D. (b) Influences of H on MFPT for different D. (c) The single trajectory of particles when escaping from the bottleneck for $D = 0.25$, $H = 0.3$ and 0.7. (d) The single trajectory of particles when escaping from the bottleneck for $D = 1$, $H = 0.3$ and 0.7.

section, the influence mechanism of H on v, P_{st}, and MFPT are analyzed in detail.

At first, relationships between H and v are calculated, as shown in Fig. 7(a). First, for cases $H > 0.5$, the smaller H, the larger v is, and the larger H, the smaller v is. This result can be explained by means of $S(f)$. As shown in Sec. II B, in the persistence case, there are more low-frequency components in FGN, which can result in a long excitation time. Particles will get enough energy from this long time to move large distances substantially, and the number of collisions with channel walls increase. Thus, v decreases. However, H is not the only factor determining v. Especially for cases $H < 0.5$, the influence mechanism of H on v is also affected by D. When $D = 1$, the impact mechanism is relatively simple and monotonously decreasing. In this case, although the high-frequency component in FGN is large and the excitation time is short, but D is sufficiently large, most particles can still have enough energy to move long distances in $w(x)$, and thus more collisions happen which can lead to a decrease of v. Moreover, with the increase of H, the excitaion time is longer and collisions become more frequently. Therefore, v is smaller as H is increasing. However, when $D = 0.25$, the influence mechanism of H on v is complicated. It tends to decrease first, then increase to a maximum at $H = 0.5$, and finally decrease. The result at $D = 0.4$ exhibits a similar change behavior as $D = 0.25$, but the change magnitude is smaller. That is, FGN tends to promote particle transport at a very small H. When H continues to increase, the promoting effect gradually weakens and disappears, eventually transforms into the inhibitory effect. The interpretation of this phenomenon is as follows. For the part that v is decreasing, the influence mechanism of H is the same as for $D = 1$. But there are only some particles having enough energy to successfully move along $w(x)$, which leads to a small v. For the part that v is increasing, it is mainly because the increase of the excitation

time induces more particles to get enough energy to move in the right direction. In addition, similar to Fig. 4, due to the existence of F and $w(x)$ with a reflection condition, v in Fig. 7(a) does not approach 0 as H tends to 0.

In Fig. 7(b), relationships between H and MFPT are discussed under $D = 0.25$ and 1. First, let us look at the results for $H \geqslant 0.5$. As H is increasing from 0.5, MFPT in both D values appear to increase monotonically. The larger H, the longer time it takes to cross the nearest bottleneck. That is, H has an inhibitory effect on the crossing behavior. Besides, from the slope of curves, it can be seen that the inhibition gradually becomes stronger. Second, our results at $H < 0.5$ show that the influence mechanism of H on MFPT is affected by D at the same time. When $D = 0.25$, MFPT increases first and then decreases. The MFPT for $H < 0.2$ is smaller than for $H = 0.5$. Thus, in this case, the impact of H on MFPT is as follows. H first promotes the crossing, but as it increases, this promoting effect is weakened. When H increases to a certain extent (approximately equal to 0.18 here), the promoting effect disappears, H begins to inhibit the crossing, and the inhibitory effect becomes stronger in a certain H range. When H increases to 0.3, the inhibition begins to weaken. However, when $D = 1$, H always prevents the crossing. In addition, the slope of MFPT demonstrates that the inhibitory effect is first enhanced and then weakened.

Here, the single trajectory for different D is also given in Figs. 7(c) and 7(d) to explain the effect of H on the MFPT. Figure 7(c) shows the influence of H for $D = 0.25$. When $H = 0.7$, the trajectory remains between its initial position and the bottleneck in the right side, and the direction of the movement is always to the right, thereby the particle can reach the bottleneck and escape in a very short time. However, when $H = 0.3$, the trajectory fills the space, and the moving direction constantly changes. Thus compared to $H = 0.7$, the time the particle spends inside of $w(x)$ and the time it takes to reach one bottleneck is longer for $H = 0.3$. This is consistent with the result in Fig. 7(b). Figure 7(d) shows the trajectory for $D = 1$. Similar to Fig. 6(a), the displacement at each time step for $H = 0.3$ is larger than for $H = 0.7$. Therefore, the time required for $H = 0.3$ to escape is shorter than for $H = 0.7$.

Figure 8 shows the distribution of the final position $\{x_n(t)\}_{1\leqslant n\leqslant N}$ for different H. Figures 8(a) and 8(b) are distribution probabilities at $D = 0.25$. In Fig. 8(a), when H changes from 0.1 to 0.4, the peak of P_{st} shifts to left and then turns to right. A left shifted distance leads to a decrease of v and inversely a right directed shift means an increase of v. This explains the phenomenon shown in Fig. 7(a). In Fig. 8(b), an increase of H contributes to a left directed shift of the peak, which equaling to the decrease of v. Meanwhile, distances of left directed shift keep the same for every increase of H. So, for $H > 0.5$ in Fig. 7(a), v is approximately proportional to H. Figures 8(c) and 8(d) are distributions under $D = 1$. When H increases, the peak of P_{st} turns to move in the left direction, which explains the monotonically decreasing behavior of v in Fig. 7(a). Another interesting phenomenon shown in Fig. 8 is that, when H increases between (0,1), the shape of P_{st} changes from chunky to thin and finally becomes chunky again. In other words, when H is large enough to 1 or small enough to 0, the positions of the particles at the final state are more dispersed, and when the intermediate value of H is taken, the distributions of the particles at the final state are more concentrated. Table II summarizes the main findings of this part.

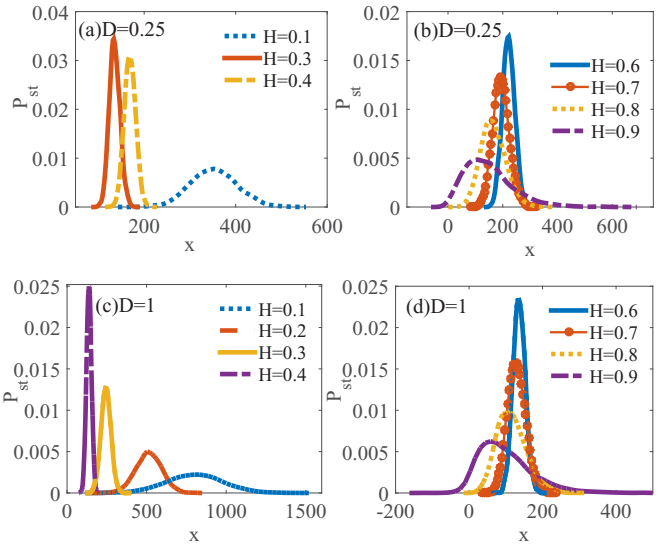

FIG. 8. Influences of H on the P_{st}.

IV. INFLUENCES OF DEFORMABLE CHANNEL

By means of increasingly sophisticated growth methods, a cross section of a channel can be modulated along its axis and this enables one to organize channels fabricated from asymmetric unit cells and diverse geometries [52]. As a result, studies about the transport in such confined structures are essential. In this section, transport properties and escape under different channel structures in the presence of FGN are studied, mainly including effects of channel bottleneck (Sec. IV A) and channel asymmetry (Sec. IV B).

A. Influences of the width parameter *b*

According to Sec. II C, there are two factors to regulate the width of the bottleneck, b and Δ. The parameter b regulates the width by controlling the vertical movement of the channel boundary in the y axis and only affects the width. In this part, effects of changes in b are analyzed. Δ is set to be zero.

Figure 9 shows relationships between v, MFPT and b. In Figures 9(a) and 9(b), regardless of the values of H and D, v will increase as b is increasing. For this, it can be considered that, although H affects the particle transport, the influence of

TABLE II. Summary of the influence of increased H on v, P_{st} and MFPT for different D.

	v	The peak of P_{st}	MFPT
$D=0.25$	Decrease first, then increase, and finally decrease	Move to the left, then right, and finally left	Increase first, then decrease, and finally increase
$D=0.4$	Decrease first, then increase, and finally decrease	Move to the left, then right, and finally left	
$D=1$	Decrease	Move to the left	Increase

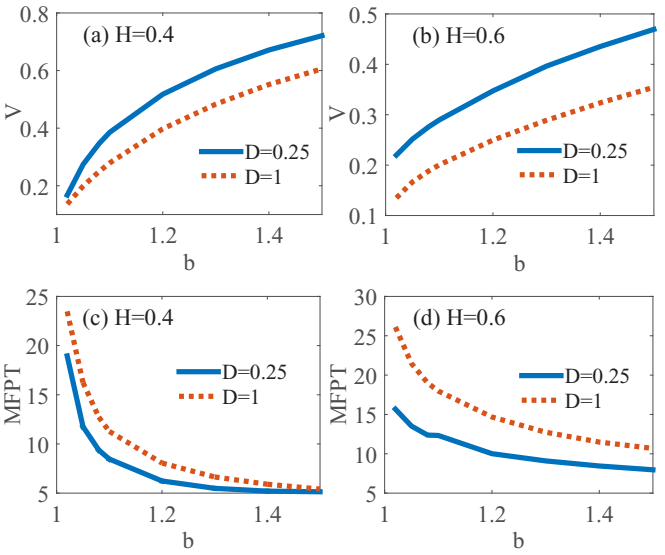

FIG. 9. Influences of b on v and MFPT for different H.

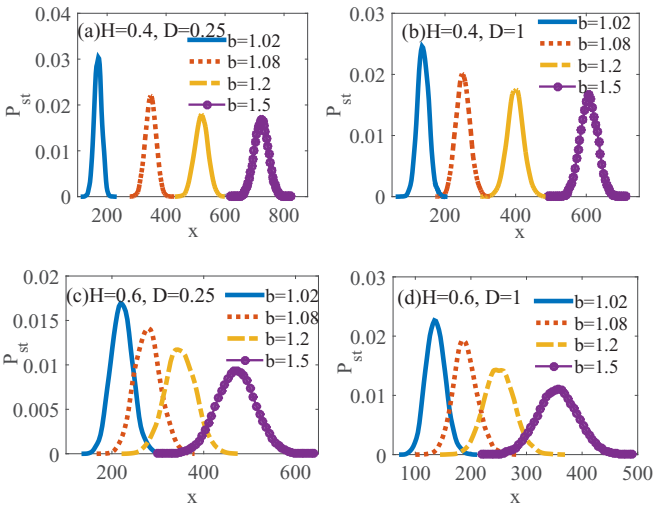

FIG. 10. Influences of b on the P_{st}.

b on the particle movement is the dominant factor. The larger b, the larger the width of the bottleneck is. The available space near the bottleneck for particles is larger, and the difficulty to pass through its vicinity becomes smaller. Thus, particles can travel a long distance in the channel and thus have a large v. Therefore, for particles, any combination of H and a large b can cause a large transport distance in the channel. Meanwhile, influences of H cannot be ignored. It can be clearly seen that v is larger at $H = 0.4$ than at $H = 0.6$. That is, in the combination of (H, b), the smaller H, the longer particles move. Influences of b on the MFPT is presented in Fig. 9(c). Similar to the former section, it is opposite to the relationship between v and b. With the increase of b, MFPT for particles to successfully cross the nearest bottleneck is decreasing. When b is increasing to a very large value, limiting to infinity, the confined space composed of two channel boundaries and the width of the bottleneck are infinite. Then it can be approximately considered that the transport of particles is no longer affected by $w(x)$. Therefore, for systems with confinement, the existence of $w(x)$ prevent the transporting and crossing behaviors. The inhibitory effect weakens as b is increasing. In addition, our results for $b = 1.4$ and 1.5 indicate that when b reaches a certain threshold, the obstruction effect is basically unchanged and can be neglected.

For a better understanding of the influence mechanism of b, the distribution P_{st} of final position is given in Fig. 10. Our results show that as b is increasing, the peak of P_{st} always shifts to the right. That is, for a larger b, most of the particles locate in a far position, and contribute to a larger v. Besides, comparing Figs. 10(a) and 10(c), under the same b and D, the peak of P_{st} also depends on H. When $b = 1.02$, the peak for $H = 0.4$ locates at 170 and at 210 for $H = 0.6$. At this time, larger H results into larger v, while for $b = 1.08$, 1.2 and 1.5, the peak position for $H = 0.4$ is bigger. That is, for cases with wide bottleneck, FGN with small H does more benefit to the transport. Meanwhile, results in Figs. 10(b) and 10(d) demonstrate that the final position of particles for $H = 0.4$ is always farther than for $H = 0.6$. Therefore, properties of P_{st} verify the conclusion that a combination of larger b and smaller H is a prominent choice. Table III summarizes the main findings of this part.

B. Influences of the asymmetric parameter Δ

Channels under different Δ in Fig. 2(a) show that, when Δ changes from 0 to nonzero, $w(x)$ varies from symmetric to asymmetric and the bottleneck becomes narrow. Thus, when Δ varies, both the bottleneck and the channel asymmetry affect the particle movement simultaneously. Here, the influence mechanism of these two aspects induced by changing of Δ is analyzed.

Figure 11 plots v-Δ curves for different H. Our results indicate that v for $H = 0.4$ is larger than for 0.5. This confirms the conclusion that v increases as H decreases. As mentioned before, when $\Delta \neq 0$, $w(x)$ is asymmetric. According to Ref. [48], the asymmetry of the confinement can induce a directed transport of particles and produce a net velocity. Here, on the one hand, the channel asymmetry caused by $|\Delta|$ leads to an increase of v. On the other hand, according to the conclusion in Sec. IV B, the decrease of the bottleneck width induced by $|\Delta|$ suppresses the increase of v. The results in Fig. 11 indicate that, as $|\Delta|$ increases, v decreases. Therefore, in the process of increasing $|\Delta|$, the inhibitory effect induced by the narrow bottleneck is always the main factor. Besides, Δ in this figure is symmetric around 0. Under this value, if $H = 0.5$ and no external force acting on the particles, the symmetric structure of Δ can be reflected in v, i.e., the $v - \Delta$ curve is symmetric around $\Delta = 0$. Then when an external force is added, like $f = 1$ in this paper, it will break the original symmetry and the $v - \Delta$ curve becomes asymmetric, as shown in the dotted line. However, when the excitation changes from white noise to FGN, this asymmetry is not maintained (see the solid line in Fig. 11).

TABLE III. Summary of the influence of increased b on v, P_{st}, and MFPT.

	v	The peak of P_{st}	MFPT
b	Increase	Move to the left	Decrease

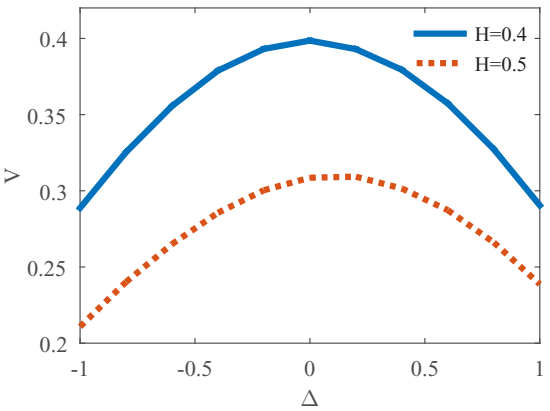

FIG. 11. Influences of Δ on v for different H at $D = 1$, $b = 1.2$.

V. CONCLUSION

Herein, we study the transport and escape in systems confined by a deformable channel under the excitation of FGN. Both FGN and channel geometry play a key role in particle transport in such a system. The coherence of FGN and confinement may give rise to complex transport features. Some interesting phenomena are found in our research by calculating the mean velocity, the first passage time and the distribution of the final position as a function of system parameters, like the Hurst exponent, noise intensity of FGN or channel geometry.

At first, influence mechanisms of FGN parameters, including the Hurst exponent and noise intensity, are studied in detail. For any channel structure, a small Hurst index induces a more efficient transport and escape. For the persistence case, the mean velocity decreases monotonically as the noise intensity is increasing, which is explained by analyzing the distribution of the final position for particles. Obviously, the first passage time to crossing the nearest bottleneck decreases. For the antipersistence case, the Hurst index and noise intensity regulate the transport in the channel together. For example, when the Hurst exponent is around 0.3, the mean velocity is proportional to the noise intensity. However, when the Hurst exponent is changing from 0.3 to 0.5, and the noise intensity is increasing, the mean velocity will decrease first and then increase. Thus, under appropriate parameters, FGN can not only promote the system transport behaviors, but also prevent the motion.

Meanwhile, effects of channel shapes, consisting of width and symmetric parameter, are studied too. For any Hurst exponent, both the reduction of the width parameter and the increase of the asymmetry parameter can lead to a decrease in the width of the bottleneck, resulting in a decrease of the mean velocity and an increase of the first passage time. Thus, compared to the free environment, the existence of channel and its bottleneck hinders the transport and escape of particles. In addition, the increase of the asymmetry parameter can also destroy the symmetric balance in the channel, and thereby facilitating the transport. However, this influence is secondary, and the effect of the reduction in the width of the bottleneck is the main mechanism. On this basis, it is meaningful to select appropriate model parameters to design an equipment basing on the purpose and interpret phenomena in actual systems.

Although this paper mainly focuses on the average velocity and the first passage time in the deformable channel, the mean square displacement and the autocorrelation function of velocity and displacement are also important parameters to characterize the transport of particles. Therefore, these indicators should also be considered when studying the transport in channels, which is a future work.

ACKNOWLEDGMENTS

This work was supported by the National Natural Science Foundation of China (Grant No. 11772255), Shaanxi Project for Distinguished Young Scholars, and the Fundamental Research Funds for the Central Universities.

APPENDIX

Here, a detailed description of generating FGN random numbers are given. For different H values, we choose a corresponding suitable method.

For the antipersistent case $0 < H < 0.5$, a fast and accurate algorithm provided by Lowen and Bardet [17,18] is used. The algorithm consists of the following steps:

(1) Defining a function $R(i)$ with period $2L$,

$$R(i) = \begin{cases} \left(1 - \left(\frac{i}{L}\right)^{2H}\right)/2, & 0 \leqslant i \leqslant L \\ R(2L - i), & L < i < 2L \end{cases},$$

where H is the Hurst exponent satisfying $0 < H < 0.5$, and L is the needed sample length.

(2) Performing a discrete Fourier transformation of $\{R(i)\}$,

$$\mathcal{R}(k) = \mathcal{F}\{R(i)\}.$$

(3) Generating another series $\{X(k)\}$ satisfying

$$X(k) = \begin{cases} 0, & k = 0 \\ \sqrt{\frac{\mathcal{R}(k)}{2}}(G_1(k) + iG_2(k)), & 1 \leqslant k \leqslant L - 1 \\ \sqrt{\mathcal{R}(k)}\nu, & k = L \\ X^*(2L - k), & L < k < 2L \end{cases},$$

where ν, G_1, and G_2 are i.i.d. standard Gaussian random numbers and $*$ represents the complex conjugate operation.

(4) Computing the inverse Fourier transformation of $\{X(k)\}$, denote as $\mathcal{X}$,

$$\mathcal{X}(i) = \mathcal{F}^{-1}\{X(k)\}.$$

(5) Sample values of the FBM process $\{B_H(i)\}$ is the proportion to the difference of $\{\mathcal{X}(i)\}$, i.e.,

$$B_H(i) = \sqrt{2L}[\mathcal{X}(i) - \mathcal{X}(0)].$$

The FGN sample random number is obtained by differentiating the sample series $\{B_H(i)\}$ in step (5).

For the persistent case $0.5 < H < 1$, a circulant matrix embedding method by using the fast Fourier transform provided by Wood and Chan [16] is used here. The concrete simulation procedure is as follows.

(1) Choose an integer $I = 2^p \geqslant 2(L - 1)$. According to the correlation function Eq. (8) of FGN, define a R-dimensional

vector V with the form

$$V = \left[r(0), r(1), \ldots, \; r\left(\frac{I}{2} - 1\right), \; r\left(\frac{I}{2}\right), \right.$$
$$\left. r\left(\frac{I}{2} - 1\right), \ldots, \; r(1) \right].$$

(2) Computing the fast Fourier transform of the vector V, denoted as U,

$$U = [u(1), u(2), \ldots, u(I)] = \mathcal{F}\{V\}.$$

(3) Generating a I-dimensional random complex vector Z, satisfying

$$Z = G_1 + iG_2,$$

where G_1 and G_2 are two independent Gaussian random numbers with zero mean and unit variance.

(4) Reassigning the vector U in step (3), as follows:

$$U = [u(1), u(2), \ldots, u(I)] = \sqrt{U}Z.$$

(5) Performing a Fourier transform on U and extract the real part of the first L numbers of the transformed sequence, one obtains a L-pointed FGN sample path with the autocorrelation function Eq. (8).

[1] H. Yang, G. Luo, P. Karnchanaphanurach, T.-M. Louie, I. Rech, S. Cova, L. Xun, and X. S. Xie, Science **302**, 262 (2003).
[2] A. Caspi, R. Granek, and M. Elbaum, Phys. Rev. Lett. **85**, 5655 (2000).
[3] A. V. Weigel, B. Simon, M. M. Tamkun, and D. Krapf, Proc. Natl. Acad. Sci. USA **108**, 6438 (2011).
[4] M. Weiss, M. Elsner, F. Kartberg, and T. Nilsson, Biophys. J. **87**, 3518 (2004).
[5] A. Caspi, R. Granek, and M. Elbaum, Phys. Rev. E **66**, 011916 (2002).
[6] J.-H. Jeon, H. Martinez-Seara Monne, M. Javanainen, and R. Metzler, Phys. Rev. Lett. **109**, 188103 (2012).
[7] J.-H. Jeon, V. Tejedor, S. Burov, E. Barkai, C. Selhuber-Unkel, K. Berg-Sørensen, L. Oddershede, and R. Metzler, Phys. Rev. Lett. **106**, 048103 (2011).
[8] S. C. Weber, A. J. Spakowitz, and J. A. Theriot, Phys. Rev. Lett. **104**, 238102 (2010).
[9] G. Matheron and G. D. Marsily, Water Resour. Res. **16**, 901 (1980).
[10] S. A. Tabei, S. Burov, H. Y. Kim, A. Kuznetsov, T. Huynh, J. Jureller, L. H. Philipson, A. R. Dinner, and N. F. Scherer, Proc. Natl. Acad. Sci. USA **110**, 4911 (2013).
[11] J.-H. Jeon, N. Leijnse, L. B. Oddershede, and R. Metzler, New J. Phys. **15**, 045011 (2013).
[12] S. Havlin and D. Ben-Avraham, Adv. Phys. **36**, 695 (1987).
[13] R. Zwanzig, J. Stat. Phys. **9**, 215 (1973).
[14] B. B. Mandelbrot and J. W. Van Ness, SIAM Rev. **10**, 422 (1968).
[15] A. V. Chechkin, I. M. Zaid, M. A. Lomholt, I. M. Sokolov, and R. Metzler, Phys. Rev. E **79**, 040105(R) (2009).
[16] A. T. Wood and G. Chan, J. Comput. Graph. Stat. **3**, 409 (1994).
[17] S. B. Lowen, Methodol. Comput. Appl. Probabil. **1**, 445 (1999).
[18] J.-M. Bardet, G. Lang, G. Oppenheim, A. Philippe, and M. S. Taqqu, *Long-range Dependence: Theory and Applications* (Birkhäuser, Basel, Switzerland, 2003) pp. 579–623.
[19] A. V. Chechkin and V. Y. Gonchar, Chaos, Solitons Fractals **12**, 391 (2001).
[20] S. C. Kou and X. S. Xie, Phys. Rev. Lett. **93**, 180603 (2004).
[21] S. C. Kou, Ann. Appl. Stat. **2**, 501 (2008).
[22] H. Qian and S. C. Kou, Annu. Rev. Stat. Appl. **1**, 465 (2014).
[23] Y. Xu, B. Pei, and J. Wu, Stochast. Dynam. **17**, 1750013 (2017).
[24] B. Pei, Y. Xu, and G. Yin, Stochast. Dynam. **18**, 1850023 (2018).
[25] B. Pei and Y. Xu, Adv. Dif. Equat. **2016**, 194 (2016).
[26] M. Deng and W. Zhu, Nonlin. Dynam. **83**, 1015 (2016).
[27] I. Goychuk and P. Hänggi, Phys. Rev. Lett. **99**, 200601 (2007).
[28] O. Y. Sliusarenko, V. Y. Gonchar, A. V. Chechkin, I. M. Sokolov, and R. Metzler, Phys. Rev. E **81**, 041119 (2010).
[29] J. Jeon, A. Chechkin, and R. Metzler, Europhys. Lett. **94**, 20008 (2011).
[30] T. G. Mattos, C. Mejía-Monasterio, R. Metzler, and G. Oshanin, Phys. Rev. E **86**, 031143 (2012).
[31] W. Wang, Z. Yan, and X. Liu, Phys. Lett. A **381**, 2324 (2017).
[32] P. Gates, K. Cooper, J. Rae, and R. Eisenberg, Progr. Biophys. Mol. Biol. **53**, 153 (1989).
[33] Z. Siwy, I. D. Kosińska, A. Fuliński, and C. R. Martin, Phys. Rev. Lett. **94**, 048102 (2005).
[34] I. D. Kosińska, I. Goychuk, M. Kostur, G. Schmid, and P. Hänggi, Phys. Rev. E **77**, 031131 (2008).
[35] D. Reguera, G. Schmid, P. S. Burada, J. M. Rubi, P. Reimann, and P. Hänggi, Phys. Rev. Lett. **96**, 130603 (2006).
[36] M. H. Jacobs, *Diffusion Processes* (Springer, Berlin, 1935), pp. 1–145.
[37] R. Zwanzig, J. Phys. Chem. **96**, 3926 (1992).
[38] R. Zwanzig, Physica A: Stat. Mech. Appl. **117**, 277 (1983).
[39] D. Reguera and J. M. Rubi, Phys. Rev. E **64**, 061106 (2001).
[40] B. Palmieri and S. A. Safran, Phys. Rev. E **86**, 031111 (2012).
[41] J. Wu, Q. Chen, and B. Ai, Phys. Lett. A **379**, 3025 (2015).
[42] W. Riefler, G. Schmid, P. Burada, and P. Hänggi, J. Phys. Cond. Matter Inst. Phys. J. **22**, 454109 (2010).
[43] Y. Li, Y. Xu, W. Xu, Z. Deng, and J. Kurths, Phys. Rev. E **96**, 022152 (2017).
[44] X. Ao, P. Ghosh, Y. Li, G. Schmid, P. Hänggi, and F. Marchesoni, Eur. Phys. J.: Spec. Top. **223**, 3227 (2014).
[45] X. Wang, J. Chem. Phys. **144**, 044101 (2016).
[46] H. Ding, H. Jiang, and Z. Hou, J. Chem. Phys. **143**, 244119 (2015).
[47] M. F. Carusela and J. M. Rubi, J. Phys.: Condens. Matter **30**, 244001 (2018).
[48] B. Ai, Z. Shao, and W. Zhong, J. Chem. Phys. **137**, 174101 (2012).
[49] Y. Xu, R. Mei, Y. Li, and J. Kurths, *Stochastic Dynamics Out of Equilibrium. IHPStochDyn 2017*, Springer Proceedings in Mathematics & Statistics Vol 282 (Springer, Cham, 2019), pp. 443–456.
[50] B. Q. Ai, Y. F. He, and W. R. Zhong, Phys. Rev. E **82**, 061102 (2010).
[51] D. Holcman, N. Hoze, and Z. Schuss, Phys. Rev. E **84**, 021906 (2011).
[52] P. K. Ghosh and F. Marchesoni, J. Chem. Phys. **136**, 116101 (2012).